



Published in final edited form as:

Exp Neurol. 2020 April ; 326: 113168. doi:10.1016/j.expneurol.2019.113168.

Cuprizone-induced demyelination under physiological and post-stroke condition leads to decreased neurogenesis response in adult mouse brain

Fucheng Luo^a, Zhen Zhang^a, Austin Barnett^b, Tania Bellinger^a, Flavia Turcato^a, Kelly Schmidt^a, Yu Luo^a

^aDepartment of Molecular Genetics, Biochemistry and Microbiology, University of Cincinnati, Cincinnati, USA

^bDepartment of Neurological Surgery, Case Western Reserve University, Cleveland, USA

Abstract

Due to the limitation in treatment window of the rtPA (recombinant tissue plasminogen activator), the development of delayed treatment for stroke is needed. We previously reported that there is a difference in neurogenesis and neuroblast migration patterns in different mouse stroke models (proximal and distal middle cerebral artery occlusion models, pMCAo or dMCAo). Specifically, compared to robust neurogenesis and substantial migration of newly born neuroblasts in pMCAo model, dMCAo only illicit limited neurogenesis and migration of neuroblasts towards ischemic area. One potential reason for this difference is the relative location of ischemic area to white matter and the neurogenic niche (subventricular zone, SVZ). Specifically, white matter could serve as a physical barrier or inhibitory factor to neurogenesis and migration in the dMCAo model. Given that a major difference in human and rodent brains is the content of white matter in the brain, in this study, we further characterize these two models and test the important hypothesis that white matter is an important contributing inhibitory factor for the limited neurogenesis in the dMCAo model. We utilized a genetically inducible NSC-specific reporter mouse line (nestin-CreERT2-R26R-YFP) to label and track NSC proliferation, survival and differentiation in ischemic brain. To test whether myelin is inhibitory to neurogenesis in dMCAo model, we demyelinated mouse brains using cuprizone treatment after stroke and examined whether there is enhanced neurogenesis or migration of neuroblasts cells in stroke mice treated with cuprizone. Our data suggests that demyelination of the brain does not result in enhanced neurogenesis or migration of neuroblasts, supporting that myelin is not a major inhibitory factor for stroke-induced neurogenesis. In addition, our results suggest that in non-stroke mice, demyelination causes decreased neurogenesis in adult brain, indicating a potential positive role of myelin in maintenance of adult neural stem cell niche.

Keywords

Proximal MCAo; Distal MCAo; Stroke; Neurogenesis; White matter

Disclosures
None.

1. Introduction

Even with the improvement of the [therapeutic window](#) in [thrombectomy](#) treatment of stroke, the treatment window for stroke is still limited to 6–24 h after stroke (Powers et al., 2018). In addition, the percentage of patient receiving tPA treatment or recannulation is <10% (Powers et al., 2018; Jadhav et al., 2018; Mendez et al., 2018). Therefore, there is still urgent need to develop treatment strategies in subacute or chronic stage for stroke patients. It has been demonstrated that the rodent brains have the capacity to repair after stroke (Luo, 2011; Carmichael, 2008). Many studies have demonstrated that stroke can activate neurogenesis in the subventricular zone (SVZ) and subgranular zone (SGZ) (Jin et al., 2001; Arvidsson et al., 2002; Parent, 2003) in animal stroke models. Ablation of the [doublecortin](#) (DCX) positive neuroblast cells suppresses adult neurogenesis and attenuates recovery of motor function after stroke (Jin et al., 2010; Sun et al., 2012). These studies supports the importance of adult neurogenesis in the functional recovery following stroke. Recent studies suggest that the human brain also harbors [neural stem cells](#) (NSCs) in the SVZ. Both the [hippocampus](#) as well as the striatum have ongoing neurogenesis (Ernst et al., 2014; Spalding et al., 2013). However, whether adult neurogenesis plays a critical role in stroke recovery in human is unknown. Some important differences between human brains and rodent brains, such as the differences in white matter percentage (Ventura-Antunes et al., 2013; Miller et al., 1980), might affect the translation of preclinical rodent models to future human therapy development. Currently, there are several different types of rodent stroke models in preclinical animal study. These different animal stroke models mimic different subtypes of stroke in humans and direct comparison of these models in detail regarding behavioral functional outcome and neurogenesis patterns have not been carried out previously. The proximal middle cerebral artery occlusion (MCAo) and distal MCAo model differ significantly concerning the size and location of the infarct in the brain. Our data showed that due to these differences, behavioral outcomes vary in these two models. In this study, for the first time, we compared neurogenesis pattern in stroke brain in these two models utilizing the nestin-CreERT2-R26R-YFP mice and identified very different neurogenesis responses and patterns in these two models. Furthermore, given the major difference between human and rodent brains in the sense of white matter content and location, we also tested the important hypothesis whether white matter/myelin is a major inhibitory factor for neurogenesis and migration of neuroblasts after stroke.

2. Materials and methods

2.1. Animals

All animal protocols were conducted under National Institutes Health (NIH) Guidelines using the NIH handbook *Animals in Research* and were approved by the Institutional Animal Care and Use Committee (University of Cincinnati). The mice were housed in the animal facility of University of Cincinnati on a 12-h light/dark diurnal cycle. Food was provided ad libitum. To evaluate neurogenesis in stroke mice, the nestin-CreERT2-R26R-YFP strain was used in this study. The generation and characterization of animals used in this study were previously described (Lagace et al., 2007; Jin et al., 2015).

2.2. Murine model of transient focal ischemia

Transient MCAo was induced in C57BL/6 or Nestin-CreERT2-YFP mice (C57BL/6 congenic background, 10–12 week old) mice as described (Longa et al., 1989). Transient MCAo was induced by an intraluminal suture method. Mice were anesthetized with isoflurane and a midline neck incision was made to expose the right common carotid artery (rCCA). The isolated rCCA was temporarily ligated with a silk suture during whole period of occlusion. The right external carotid artery (rECA), and the right internal carotid artery (rICA) were also isolated by dissection of fascia. The rICA was clamped with an artery clamp above a loose suture tie around rICA. The rECA was ligated and cut to make a rECA stump. A nylon filament suture with a silicone rubber-coated tip (#602212PK10Re, Docol co, Sharon, MA, USA) was inserted in rECA stump and further pushed along the lumen of ICA while the clamp was released and then the tie around rICA was tightened. After 45 min of occlusion, the nylon suture was gently removed from rMCA to reperfuse the rMCA territory. The rECA stump was permanently ligated and the temporary ligation in rCCA and rICA were removed to allow normal blood flow to the brain. During the surgery, mice were placed above a temperature-controlled heating blanket and after the 45 min occlusion, the skin wound was closed with suture and the mice were placed in a heated animal intensive care unit chamber until recovery. To ensure consistent and successful blockage of MCA, we monitored ischemia in all of our animals by Laser Doppler flowmetry (PeriFlux System 5000, Perimed, Järfälla-Stockholm, Sweden).

2.3. Cortical ischemia model (distal MCA occlusion)

Focal cerebral ischemia was produced in the mice as described in detail previously (Shen et al., 2008; Luo et al., 2009). The mice were anesthetized with chloral hydrate (0.4 g/kg, intraperitoneally [IP]). Body temperature was monitored and maintained at 37 °C by a heating pad. The surgical area was shaved and prepared with alternating betadine scrub and ethanol. A small 5-mm vertical skin incision was cut between the right eye and ear to expose the skull. A craniotomy of about 1 × 1 mm² was made in the right squamosal bone to expose the middle cerebral artery (MCA). The MCA was ligated with 10–0 suture for 90 min followed by removal of the ligating suture at right CCA to allow for partial reperfusion. The skin wound was closed with suture and the mice were placed in a heated animal intensive care unit chamber until recovery. After recovery from the anesthesia, body temperature was maintained at 37 °C using a temperature-controlled incubator.

2.4. Tamoxifen administration

Male nestin-CreERT2-R26R-YFP mice (8–10 weeks old) were given tamoxifen (TAM) dissolved in 10% EtOH/90% sunflower oil by gavage feeding at a dose of 180 mg/kg daily for 5 consecutive days. This dosing regimen was previously demonstrated to provide maximal recombination with minimal mortality and successfully monitored the activated SVZ NSCs by stroke (Lagace et al., 2007; Jin et al., 2015; Li et al., 2010). For NSC fate mapping, TAM treated mice received MCAo surgery 10 days after the last TAM administration and mice were perfused at 42 days post stroke to harvest the brain for immunostaining. The time frame was chosen to specifically label NSCs in adult mice before the introduction of MCAo but also allow the clearance of TAM from mice at the time of

MCAo to prevent labeling of reactive astrocytes which also upregulate nestin expression after stroke.

2.5. Transient demyelination by cuprizone treatment

Adult male C57BL/6 mice (sham or 1 week after stroke) at about 12 weeks of age were fed with 0.2% cuprizone (TD.140800, ENVIGO) for 5 weeks. Starting at 3th weeks, substantial demyelination in the corpus callosum can be observed (Matsushima and Morell, 2001). Demyelination reaches a maximum at 5 weeks (Steelman et al., 2012; Gudi et al., 2009)

2.6. Behavioral assay

Locomotor function: Animals were placed in an Accuscan activity monitor (Columbus, OH, USA) before and at various days after MCAo for behavioral recording for 1 h as previously described (Luo et al., 2009). The monitor contained 16 horizontal and 8 vertical infrared sensors spaced 2.5 cm apart. Each animal was placed in a 42 × 42 × 31 cm Plexiglas open box for 60 min. Motor activity was calculated using the automated Versamax software (Accuscan, Columbus, OH, USA). The following variables were measured to assess both horizontal movement and vertical movement: (A) total distance traveled (the distance, in centimeters, traveled by the animals), (B) Vertical activity (the total number of beam interruptions that occurred in the vertical sensors). This behavioral test is automatically monitored by the computer and software therefore avoided observer bias.

2.7. Adhesive removal test

To examine sensorimotor deficits, the adhesive removal test was performed on the indicated days in pre-stroke or post-stroke animals. Each mouse was placed into transparent cylinder (15 cm diameter) during a habituation period of 1 min. Thereafter, two different colored adhesive labels (2.5 mm diameter made by punch, Tough Spots) were applied with equal pressure on each mouse's forepaw. The mouse was recorded in the cylinder and scored later by observers blinded to the treatment. The time to remove the adhesive labels was scored with a maximum of 2 min. To achieve an optimum level of performance, mice were trained for 4 days before surgery to establish baseline performance.

2.8. Cylinder test

The Cylinder test was used to evaluate locomotor asymmetry in rodent models of stroke. As the animal moves within an open-top, clear plastic cylinder, its forelimb activity while rearing against the wall of the arena is recorded. Forelimb use is defined by the placement of the whole palm on the wall of the arena, which indicates its use for body support. Forelimb contacts while rearing are scored with a total of 20 contacts recorded for each animal. The number of impaired and non-impaired forelimb contacts are calculated as a percentage of total contacts.

2.9. MRI method

Imaging session was carried out at 2 days after stroke by staff that were blinded to the treatment groups. MRI studies were performed on a horizontal Bruker 9.4 T scanner with a 3-cm birdcage coil. Multi-slice, T₂-weighted, axial images were acquired using a rapid

acquisition with relaxation enhancement (RARE) sequence (Hennig et al., 1986) to quantify ischemic edema volume. Imaging parameters were: TE/TR, 15/2000 ms; RARE factor, 8; NAV, 4; matrix size, 256 × 256; slice thickness, 1 mm; number of slices, 13; field of view (FOV), 2.4 × 2.4 cm. Image reconstruction and analysis were performed offline using in-house developed, MATLAB-based (Natick, MA, USA) software. ROIs of ischemic edema volume and brain tissue were drawn from T₂-weighted images. Consequently, the percentage of ischemic edema volume was calculated.

2.10. Luxol fast blue staining

To examine demyelination in cuprizone treatment mice, brain cryosections (30 μm) were mounted on Superfrost Plus slides and stained with 0.1% luxol fast blue solution (#26681-01, Electron Microscopy Sciences) in 56 °C oven overnight. Sections were then rinsed sequentially in 95% ethanol, water and 0.05% lithium carbonate solution (#26681-04, Electron Microscopy Sciences) until the white matter sharply defined. When differentiation is complete, cryosections were dehydrated in 100% ethanol, cleared in xylene and mounted with cytooseal 60 mounting medium.

2.11. Immunohistochemistry

At different time points after stroke, mice were perfused transcardially with a solution of 4% paraformaldehyde (PFA, pH 7.2) in 0.1 M phosphate buffer (PB, pH 7.2). Brains were removed from the skull, post-fixed in 4% PFA overnight at 4 °C, and sequentially transferred to 20% and 30% sucrose in 0.1 M phosphate buffer, pH 7.2 solutions overnight. Brains were frozen on dry ice and sectioned on a cryostat to obtain coronal sections of 30 μm in thickness.

The sections were then incubated with blocking buffer for one hour. The primary antibodies were prepared in the blocking buffer and the sections were incubated in the solution overnight: anti-GFP (Green fluorescent protein) (1:1000; Invitrogen) and anti-DCX (1:500, Millipore). After incubation with primary antibody solution, the sections were washed and incubated for four hours at room temperature in diluted secondary antibody prepared with blocking solution (secondary antibody conjugated with Alexa 488 or Alexa 555, 1:1000; Life Technologies, Carlsbad, CA, USA). The slides were then washed with PB solution and cover-slipped. Images were acquired using a Leica microscope. Omission of primary or secondary antibodies resulted in no staining and served as negative controls. Group and treatment information are all blinded to image analyzer.

2.12. Quantification of SVZ and SGZ neurogenesis and migration

To quantify total newly born YFP+ progeny or newly born neuroblasts, YFP+ or DCX+ cells are outline with region of interest (ROIs) at the horn or wall of SVZ region as illustrated in Fig. 5A. Immunoreactive positive signals were analyzed by Nikon NIS-Elements software (Tokyo, Japan) on at least three sections at equivalent coronal positions in each animal. To quantify for the migration of YFP+ or DCX+ cells, the distance of YFP+ or DCX+ migrated from the horn of the SVZ was measured using NIS-Element software on the same three brain sections for each animal. To analyze the neurogenesis at SGZ in hippocampus, YFP+ cells were counted on at least three sections that contains similar coronal position of SGZ

regions. DCX+ immunoreactivity was quantified using NIS-Element software on the same three sections for each animal. The quantification results were averaged for each animal from the measured sections and used as a single data point for statistical analysis. All of the images were analyzed by observers blinded to the treatment group.

2.13. SVZ and SGZ neural stem cell 3D neurosphere growth assay

Primary stem cell cultures were obtained from C57BL/6J mice at 4–6 weeks of age from the SVZ and SGZ as described (Turcato et al., 2018; Guo et al., 2012). Whole brains were harvested and dissected under microscope to obtain the subventricular zone (SVZ) and SGZ tissue. After mechanical dissociation with a stab knife, the tissue fragments were processed using trypsin and resuspended as individual cells at a density of 10^4 cells/cm² in neurobasal media with growth factors EGF and bFGF (NBM-GF). Subsequent passaging of cells was performed using Accutase (Innovative #AT-104) every 7 days until the cells established viable lines, and cellular debris was naturally diminished after each passage. At day 4 of each passage, the proliferating spheres were fed with NBM-GF. We used NSCs at passage P3-P8 in this study. After dissociation the neurospheres during passaging, individual cells were plated at a density of 3×10^3 (Mendez et al., 2018) cells/well in a round bottom 96-well plate in 100uL of NBM-GF with vehicle or different concentrations of cuprizone treatment. After 48 h of neurosphere aggregation, neurospheres were treated with different concentrations of cuprizone or vehicle. On day 7, images of each well were taken using Evos M5000 microscope (ThermoFisher Scientific). 8 replicate wells were quantified for each condition and the radius of the neurospheres were measured using Nikon NIS Element software (Nikon). Three replicating experiments showed similar results.

2.14. Statistics

Results are expressed by mean \pm SEM of the indicated number of experiments. Statistical analysis was performed using Student's *t*-test, and one- or two-way analysis of variance (ANOVA), as appropriate, with Student-Newman-Keuls post hoc tests or Bonferroni post-hoc tests for repeated behavioral measurements. A *p*-value equal to or <0.05 was considered significant. Number of animals used in each experiments are indicated in figure legends.

3. Results

3.1. Proximal middle cerebral artery occlusion (pMCAo) and distal middle cerebral artery occlusion (dMCAo) model produce different pattern and size infarct

Both pMCAo and dMCAo are widely used in modeling ischemic stroke in rodents. We have previously observed that pMCAo and dMCAo showed different response in regards to neurogenesis (Jin et al., 2015). However, to the best of our knowledge, comprehensive and detailed comparison between these two models have not been carried out. In this study, we first examined the location and size of infarct in these two models. Both TTC staining and T2-weighted MRI showed that pMCAo induces a much larger infarct covering both striatal and cortical area and dMCAo induces a smaller infarct restricted to cortical area dorsal and lateral to the corpus callosum (Fig. 1 A–D). We used T2-weighted MRI to quantify the infarct size of pMCAo and dMCAo and the result showed that pMCAo results in an infarct

volume average of 52.23% of the hemisphere and dMCAo results in an infarct volume average of 9.31% of the hemisphere (Fig. 1E).

3.2. Proximal MCAo and distal MCAo results in different behavioral deficits in mice

Given the different pattern and size of infarct in the brain following pMCAo or dMCAo, we next examined the behavioral outcome following either pMCAo or dMCAo. Since pMCAo lead to larger infarct and more severe motor deficits, we examined the motor deficits starting from post-stroke day 3 and for dMCAo we measured post-stroke day 1 and 4 during the acute stage. Both models were followed up till 4 weeks after stroke to examine the subacute-chronic recovery in behavioral function. We first examined the locomotion activity in animals at various time point before or after stroke. This assay has been previously used by us and others to detect motor deficits in stroke animals (Luo et al., 2009; Turcato et al., 2018; Jin et al., 2017; Vahid-Ansari et al., 2016). Our results show that in mice subjected to pMCAo there are significant deficits in horizontal movement (measured by total distance traveled in 1 h in the activity chamber) as early as 3 days post stroke (Fig. 2A). There is spontaneous recovery in horizontal movement following stroke, however, the deficit is sustained until up to 4 weeks after stroke in pMCAo model (Fig. 2A). Vertical activity in pMCAo mice followed a similar trend (Fig. 2C). We then examined the locomotion activity in dMCAo mice. Since this model generates stroke infarcts that are mostly in cortical area, not affecting striatum, mice subjected to dMCAo showed significant deficits in horizontal activity during acute stages (post-stroke days 4 and 7) but animals recovered to baseline level at 2 weeks and 4 weeks after stroke (Fig. 2B). Interestingly, vertical activity demonstrated an acute decrease at 1 day after stroke but quickly recovered to baseline level at 4 days post stroke (Fig. 2D). This result suggests that the quick recovery in vertical activity might be associated with the lack of striatal lesion in the dMCAo model. We also examined **sensorimotor functions** in pMCAo or dMCAo mice using the adhesive removal test and the cylinder test. In the adhesive removal test, we observed significant deficits in all time points tested (1wk-4wk) after pMCAo model (Fig. 2E) and in the dMCAo model, a transient deficit was observed at 1 day after stroke but mice quickly recovered to baseline level in this behavioral measurement (Fig. 2F). Although dMCAo model only showed a transient deficit in the adhesive removal test, utilizing the cylinder test, we observed sustained deficits in the affected limb from 4 days to 4 weeks post stroke. The 1-day time point did not show a preference on either the unaffected or affected limb, probably due to the minimal rearing movement in stroke mice at 1 day after stroke. For the pMCAo model, depending on the infarct size (either striatal infarct or striatal + cortical infarct), the results on cylinder test was inconsistent (Data not shown).

3.3. pMCAo and dMCAo model demonstrate different pattern of neurogenesis and neuroblast migration

To compare neurogenesis and migration pattern of adult NSCs in the SVZ in the pMCAo and the dMCAo model, we utilized a previously established protocol to label and track SVZ nestin-expressing NSCs and their progeny in the nestin-Cre ERT2/R26R-YFP mice (Jin et al., 2015; Li et al., 2010; Jin et al., 2017). In a previous study, we have observed that neurogenesis patterns are different between the pMCAo and the dMCAo models (Jin et al., 2015). We have observed that there are substantially more newly born neuroblasts

migrating towards ischemic area in the pMCAo model (striatum/cortex). In contrast, there are very few DCX+ cells that demonstrated the morphology of migrating neuroblasts, and those were found along the corpus callosum (CC) but not near the cortical ischemic site (Jin et al., 2015). Using the nestin-Cre ERT2/R26R-YFP mice which allows tracking of adult SVZ derived newly born cells, we confirmed that even at 6 weeks after stroke onset, the pMCAo model exhibits substantially and significantly more newly born cells derived from the SVZ NSCs as well as more DCX+ newly born neuroblasts compared to the dMCAo model (Fig. 3A–D). We speculate that this difference in neurogenesis and neuroblasts migration can be due to several different factors. 1. Difference in the infarct size: pMCAo has significantly larger infarct compared to dMCAo. 2. Distance of the ischemic region to the SVZ niche: pMCAo leads to ischemic regions closer to SVZ region compared to dMCAo. 3. The location of ischemic region, specifically the location of infarct in regard to its relative position to white matter: pMCAo generates an infarct that is close to the SVZ and medial to the Corpus callosum (white matter) while a dMCAo generates an infarct that is further from the SVZ and lateral to the Corpus callosum (white matter). The third hypothesis is particularly interesting since one of the most prominent differences between human and rodent brains is the content of white matter and the cortical area lateral to white matter (Ventura-Antunes et al., 2013; Miller et al., 1980; Semple et al., 2013). Therefore, in this study we focused to examine whether **myelin** or white matter would be a contributing inhibitory factor for the limited neurogenesis or migration of newly born cells in the dMCAo model.

3.4. Demyelination of the mouse brain utilizing the cuprizone treatment

To examine whether the myelin/white matter might serve as a critical inhibitory factor for neurogenesis and migration of newly born cells in adult brain, we applied cuprizone treatment in sham or stroke mice. Cuprizone is a potent **chelator** of copper and has been widely used for examining demyelination/remyelination processes in **multiple sclerosis** research. Oral cuprizone treatment can demyelinate the brain in the corpus callosum adjacent to the SVZ and the cortical ischemic area (Steelman et al., 2012; Gudi et al., 2009; Praet et al., 2014). Mice were treated with **Tamoxifen** to induce the reporter expression (YFP) in adult NSCs at 10 days before the surgery. And one week after the dMCAo, we treated mice with diet containing either vehicle or cuprizone (0.2% in diet). Fast blue staining (Fig. 4) confirmed that cuprizone treatment for 5 weeks was effective in demyelinating the corpus callosum, which is consistent with previous studies (Steelman et al., 2012; Gudi et al., 2009)

3.5. Effect of demyelination on SVZ neurogenesis and neuroblasts migration in sham or stroke mice

After cuprizone treatment, we examined the number of SVZ YFP+ cells which contains NSCs and their progeny. We examined YFP+ cells both at the horn of the SVZ and the lateral wall of the SVZ, as illustrated in Fig. 5A. We found that in sham mice, cuprizone treatment led to significant decreased YFP+ cells in both the SVZ horn and SVZ wall. This suggests that cuprizone treatment lead to decreased NSCs or their progeny in non-stroke mice. Interestingly, in stroke mice, cuprizone-treated mice have similar level of YFP+ cells in both SVZ horn and wall compared to vehicle treated stroke mice, suggesting that NSCs in

stroke mice are resistant to cuprizone treatment. However, we did not observe any enhanced neurogenesis in stroke mice after demyelination with cuprizone (Fig. 5). Examining the migration of newly born cells at the SVZ by measuring the length they migrated out of the SVZ and towards the cortical area, our data showed that stroke induced more migration of YFP+ cells towards the cortex but there is no difference between the vehicle or cuprizone treated mice. This data suggests that the **microenvironment** of post-stroke brain provided factors that activated the NSCs which compensated for the decreased YFP+ cells in sham mice, and that demyelination in the stroke brain does not further enhance the expansion or migration of the SVZ NSCs (Fig. 5).

To specifically examine newly born cells that are committed to the neuronal **lineage**, we also quantified the number and migration of DCX+ neuroblast cells in the SVZ zone in sham or stroke mice treated with vehicle or cuprizone (Fig. 6). DCX+ positive cells in the SVZ horn in stroke mice has a trend of increase ($p = .06$) and migrate significantly further compared to non-stroke mice ($p < .01$). Similarly, there is no difference in DCX+ cells numbers at the SVZ horn nor at the SVZ wall in vehicle treated or cuprizone treated mice (Fig. 6 A, B). Migration distance from the SVZ horn is similar in vehicle-treated or cuprizone-treated mice (Fig. 6C). Interestingly, in sham animals, cuprizone treatment does not affect the total number of DCX+ cells, in contrast to significantly decreased YFP+ cells, suggesting that at SVZ, cuprizone treatment might affect specific populations of NSC niche cells other than mature DCX+ neuroblasts.

3.6. Effect of demyelination on SGZ neurogenesis and neuroblasts migration in sham or stroke mice

The SGZ in the hippocampus is the other main niche for adult neurogenesis the brain. Next, we examined the effect of cuprizone on both YFP+ cells and DCX+ positive cells in the SGZ. Our results showed that total YFP+ cells at the SGZ increased in stroke mice suggesting enhanced neurogenesis after stroke (Fig. 7 A/C and Fig. 7 G/I), consistent with previous studies from our and other labs. Interestingly, Cuprizone treatment almost completely abolished both YFP+ and DCX+ cells in the SGZ in non-stroke mice (Fig. 7D). In stroke mice that were treated with cuprizone, YFP+ cells are partially restored (Fig. 7J) suggesting that stroke-activated SGZ NSCs are partially resistant to cuprizone treatment; however, they fail to differentiate to neuroblast since DCX+ cells are still abolished in both non-stroke and stroke animals (Fig. 7E/F and Fig. 7K/L). This suggests a diminished capacity of these cells in **neuronal differentiation**, which is consistent with the **astrocyte** morphology of remaining YFP+ cells (Fig. 7).

3.7. Direct effect of cuprizone on SVZ and SGZ neural stem cell growth in vitro

To examine whether the decreased neurogenesis in vivo is due to direct toxicity of cuprizone to neural stem cells or an indirect effect due to demyelination, we established primary adult neural stem cell cultures from either SVZ or SGZ area. We analyzed the growth of NSCs in a 3-D neurosphere culture format to quantify the proliferation capacity of neural stem cells. Three thousand single neural stem cells from either SVZ or SGZ were plated in each single 96-well plate well which aggregate into a single neurosphere in 48 h. Cuprizone treatment was initiated at 48 h after plating to evaluate its effect on neurosphere growth. There is no

reported measurement of serum concentration of cuprizone concentration in the in vivo diet cuprizone model, therefore we used a range of concentration of cuprizone that has been shown to cause oligodendrocytes toxicity in vitro (250 μ M to 1 mM) (Benardais et al., 2013; Taraboletti et al., 2017). Our data show that all three cuprizone concentrations (250 μ M, 500 μ M and 1 mM) cause decreased neurosphere growth with higher cuprizone concentration showing more severe inhibition in neurosphere growth (Fig. 8). However, compared to the substantial decrease of YFP+ NSCs in vivo, the degree of inhibition after 7 days is moderate (10.4%-22.4% decrease). In addition, although in vivo SVZ and SGZ NSCs showed different vulnerability to cuprizone treatment, in vitro cuprizone treatment showed similar inhibitory effect in both SVZ and SGZ NSCs (Fig. 8, no significant differences between SVZ and SGZ cells in treatment groups). In summary, these data suggest that in vivo cuprizone treatment could be due to combined direct toxicity of cuprizone to NSCs and indirect effects of demyelination in the neurogenic niches.

4. Discussion

Pre-clinical stroke research has not been very successful in translating to clinical therapy (Fisher et al., 2009). A potential contributing factor is the difference between human brains and the rodent brains (Dirnagl and Endres, 2014). One of the most significant differences between human brains and rodent brains is the proportion of white matter to gray matter. Gray matter is composed of neural cell bodies, axon terminals, and dendrites. White matter is composed of axonal bundles coated with myelin. In primate and human brain, white matter composes 40–50% of the brain (Miller et al., 1980) while in rodents this percentage is only about 10% (Ventura-Antunes et al., 2013). We have previously reported (Jin et al., 2015) and in this study in further detail characterized the differences in neurogenesis and neuroblast cell migration in the pMCAo model and the dMCAo model. Besides differences in size of infarct in these two models, another important difference in the infarct location is their relative locations to white matter (corpus callosum, CC) in mouse brain. In pMCAo, the infarct area is adjacent to the SVZ and not separated by the CC. However, in dMCAo, the infarct area is mostly in the cortical area, lateral to the CC and separated from the SVZ by the CC. Given the important difference between human and rodent brains in white matter content in the human brain, we asked some critical questions: Is white matter a major inhibitory factor to neurogenesis and neuroblasts migration? Does white matter contribute to the differences we reported here in neurogenesis patterns in pMCAo and dMCAo models? Answers to these important questions will help provide evidence to evaluate whether promoting neurogenesis after stroke might be a reasonable strategy to human stroke recovery and the types of stroke that it might be suitable for. That is, if white matter is a major inhibitory factor for neurogenesis, then a cortical stroke that is separated from the SVZ by white matter might not be a good target for neurogenesis-promoting therapy. While on the other hand, a basal ganglia stroke which is adjacent to the SVZ might be a better subtype of stroke to enhance neurogenesis as a therapeutic strategy. With this important question and rationale, we first further characterized the infarct size, location, behavioral deficits and neurogenesis pattern in these two models. To our best knowledge, the direct, detailed and comprehensive comparison of these two models in mice has not been carried out previously. More importantly, utilizing the Nestin-creERT2-YFP

mice which allows us to precisely turn on a reporter gene in adult NSCs at certain time point (10 days before stroke in adult mouse) allows us to precisely label and track the adult NSCs and their progeny. Utilizing this mouse model, we further characterized and confirmed the difference in neurogenesis patterns in pMCAo model and dMCAo model. Indeed, the pMCAo model elicits a much more substantial neurogenesis response and results in more and further migration of neuroblasts cells into the infarct area than dMCAo. We then tested whether white matter is a major inhibitory factor to the limited neurogenesis and migration of neuroblast cells in the dMCAo model by demyelinating the brain at from 1 to 6 weeks after stroke. After demyelination of the brain (5 weeks after cuprizone treatment), we examined the total number of YFP+ cells and DCX+ cells and their migration distance in the dMCAo model. Our data showed that even after demyelination of the brain, we did not observe substantially increased neurogenesis of YFP+ cells nor DCX+ neuroblasts migration. On the contrary, our data suggested that in sham-operated mice, cuprizone treatment substantially decreased the total number of YFP+ cells at both the SVZ and the SGZ and it almost completely abolished the SGZ DCX+ cells. Interestingly, in stroke mice, this decrease in YFP+ cells are partially rescued, suggesting that stroke activates certain molecular pathways within NSCs or in the [microenvironment](#), which partially protected NSCs from cuprizone treatment. Our data suggest that myelin may not be a major inhibitory factor for neurogenesis and neuroblasts migration. This negative result is important because it suggests that modulating neurogenesis could be a potential therapeutic strategy despite the high content of white matter in human brain. Recently the effect of demyelinating agents such as cuprizone on the maintenance and [homeostasis](#) of adult NSCs have been suggested by other studies (Abe et al., 2015; Hillis et al., 2016). Our study also suggests that the SVZ and the SGZ might have different sensitivity to demyelinating agents. Recently, another independent study reported differences in sensitivity of SVZ and SGZ NSCs to cuprizone treatment which is consistent with our finding (Zhang et al., 2019). The observed differences in vulnerability to cuprizone treatment in SVZ and SGZ NSCs could be due to several potential reasons. Firstly, although both SVZ and SGZ niches contains adult NSCs that can differentiate into multiple [lineage](#) cells in adult brain. They are intrinsically heterogeneous. SVZ NSCs give birth to [olfactory bulb interneurons](#) and corpus callosum [oligodendrocytes](#), whereas SGZ NSCs give rise to new neurons and astrocytes in hippocampus (Bond et al., 2015). Morphologically SVZ and SGZ NSCs and their progenies are different and cell markers that identify different populations of NSCs /progenies are different at the two niches as well. During aging, SGZ neurogenesis capacity decreases more severely than SVZ neurogenesis, indicating that SGZ NSCs might be intrinsically programmed to have less capacity for prolonged self-renew and proliferation or be more vulnerable to changes in the microenvironment of the niche (Jin et al., 2004; Jin et al., 2003). These intrinsic differences between the SVZ and SGZ cells might account for increased vulnerability of SGZ NSCs to cuprizone treatment. Secondly, cuprizone induces distinct pattern of demyelination in different brain areas (Taraboletti et al., 2017; An et al., 2019). Demyelination of the hippocampus is prominent in the cuprizone model. Striatum, where the SVZ NSCs is located adjacently is less demyelinated compared to the hippocampus where the SGZ NSCs resides. This could contribute to the increased decline in neurogenesis in SGZ as well. To examine whether cuprizone could lead to direct cytotoxicity in adult SVZ and SGZ NSCs, we obtained in vitro primary NSCs cultures from adult mouse brain.

Using different cuprizone concentration in culture media that has previously been shown to cause toxicity in oligodendrocytes (Benardais et al., 2013; Taraboletti et al., 2017), we found that cuprizone treatment could directly inhibit the growth of neurospheres formed by both SVZ and SGZ NSCs. Interestingly, the direct inhibitory effect of cuprizone on SVZ and SGZ NSCs in vitro is moderate (10.4%-22.4% decrease compared to vehicle-treated neurospheres) and dose not significantly differ between SVZ and SGZ NSCs (Fig. 8). Therefore, our data suggest that in addition to direct inhibitor effect, demyelination induced indirect effects on NSCs might also contribute to the observed substantial decrease in neurogenesis in vivo. Precise mechanisms of the direct and indirect inhibitory effects of cuprizone on SVZ and SGZ neurogenesis warrants further investigation in future studies.

Sources of funding

This study is funded by NIH Grants (R01NS091213 and NS107365).

References

- Abe H, Tanaka T, Kimura M, Mizukami S, Saito F, Imatanaka N, Akahori Y, Yoshida T, Shibutani M, 2015. Cuprizone decreases intermediate and late-stage progenitor cells in hippocampal neurogenesis of rats in a framework of 28-day oral dose toxicity study. *Toxicol. Appl. Pharmacol* 287 (3), 210–221. 10.1016/j.taap.2015.06.005. [PubMed: 26057786]
- An J, Yin JJ, He Y, Sui RX, Miao Q, Wang Q, Yu JZ, Yu JW, Shi FD, Ma CG, Xiao BG, 2019. Temporal and spatial dynamics of astroglial reaction and immune response in cuprizone-induced demyelination. *Neurotox. Res* 10.1007/s12640-019-00129-4.
- Arvidsson A, Collin T, Kirik D, Kokaia Z, Lindvall O, 2002. Neuronal replacement from endogenous precursors in the adult brain after stroke. *Nat. Med* 8 (9), 963–970. 10.1038/nm747. [PubMed: 12161747]
- Benardais K, Kotsiari A, Skuljec J, Koutsoudaki PN, Gudi V, Singh V, Vulinovic F, Skripuletz T, Stangel M, 2013. Cuprizone [bis(cyclohexylidenehydrazide)] is selectively toxic for mature oligodendrocytes. *Neurotox. Res* 24 (2), 244–250. 10.1007/s12640-013-9380-9. [PubMed: 23392957]
- Bond AM, Ming GL, Song H, 2015. Adult mammalian neural stem cells and neuro-genesis: five decades later. *Cell Stem Cell* 17 (4), 385–395. 10.1016/j.stem.2015.09.003. [PubMed: 26431181]
- Carmichael ST, 2008. Themes and strategies for studying the biology of stroke recovery in the poststroke epoch. *Stroke* 39 (4), 1380–1388. 10.1161/STROKEAHA.107.499962. [PubMed: 18309162]
- Dirnagl U, Endres M, 2014. Found in translation: preclinical stroke research predicts human pathophysiology, clinical phenotypes, and therapeutic outcomes. *Stroke*. 45 (5), 1510–1518. 10.1161/STROKEAHA.113.004075. [PubMed: 24652307]
- Ernst A, Alkass K, Bernard S, Salehpour M, Perl S, Tisdale J, Possnert G, Druid H, Frisen J, 2014. Neurogenesis in the striatum of the adult human brain. *Cell* 156 (5), 1072–1083. 10.1016/j.cell.2014.01.044. [PubMed: 24561062]
- Fisher M, Feuerstein G, Howells DW, Hurn PD, Kent TA, Savitz SI, Lo EH, Group S, 2009. Update of the stroke therapy academic industry roundtable preclinical recommendations. *Stroke* 40 (6), 2244–2250. 10.1161/STROKEAHA.108.541128. [PubMed: 19246690]
- Gudi V, Moharregg-Khiabani D, Skripuletz T, Koutsoudaki PN, Kotsiari A, Skuljec J, Trebst C, Stangel M, 2009. Regional differences between grey and white matter in cuprizone induced demyelination. *Brain Res.* 1283, 127–138. 10.1016/j.brainres.2009.06.005. [PubMed: 19524552]
- Guo W, Patzlaff NE, Jobe EM, Zhao X, 2012. Isolation of multipotent neural stem or progenitor cells from both the dentate gyrus and subventricular zone of a single adult mouse. *Nature protocols* 7 (11), 2005–2012. 10.1038/nprot.2012.123. [PubMed: 23080272]

- Hennig J, Nauwerth A, Friedburg H, 1986. RARE imaging: a fast imaging method for clinical MR. *Magn. Reson. Med* 3 (6), 823–833 [PubMed: 3821461]
- Hillis JM, Davies J, Mundim MV, Al-Dalahmah O, Szele FG, 2016. Cuprizone demyelination induces a unique inflammatory response in the subventricular zone. *Journal of neuroinflammation* 13 (1), 190. 10.1186/s12974-016-0651-2. [PubMed: 27550173]
- Jadhav AP, Desai SM, Kenmuir CL, Rocha M, Starr MT, Molyneaux BJ, Gross BA, Jankowitz BT, Jovin TG, 2018. Eligibility for endovascular trial enrollment in the 6- to 24-hour time window: analysis of a single comprehensive stroke center. *Stroke*. 49 (4), 1015–1017. 10.1161/STROKEAHA.117.020273. [PubMed: 29581344]
- Jin K, Minami M, Lan JQ, Mao XO, Bateur S, Simon RP, Greenberg DA, 2001. Neurogenesis in dentate subgranular zone and rostral subventricular zone after focal cerebral ischemia in the rat. *Proceedings of the National Academy of Sciences of the United States of America* 98 (8), 4710–4715. 10.1073/pnas.081011098. [PubMed: 11296300]
- Jin K, Sun Y, Xie L, Bateur S, Mao XO, Smelick C, Logvinova A, Greenberg DA, 2003. Neurogenesis and aging: FGF-2 and HB-EGF restore neurogenesis in hippocampus and subventricular zone of aged mice. *Aging Cell* 2 (3), 175–183. 10.1046/j.1474-9728.2003.00046.x. [PubMed: 12882410]
- Jin K, Galvan V, Xie L, Mao XO, Gorostiza OF, Bredesen DE, Greenberg DA, 2004. Enhanced neurogenesis in Alzheimer's disease transgenic (PDGF-APP^{Sw,Ind}) mice. *Proceedings of the National Academy of Sciences of the United States of America* 101 (36), 13363–13367. 10.1073/pnas.0403678101. [PubMed: 15340159]
- Jin K, Wang X, Xie L, Mao XO, Greenberg DA, 2010. Transgenic ablation of doublecortin-expressing cells suppresses adult neurogenesis and worsens stroke outcome in mice. *Proceedings of the National Academy of Sciences of the United States of America* 107 (17), 7993–7998. 10.1073/pnas.1000154107. [PubMed: 20385829]
- Jin Y, Raviv N, Barnett A, Bambakidis NC, Filichia E, Luo Y, 2015. The shh signaling pathway is upregulated in multiple cell types in cortical ischemia and influences the outcome of stroke in an animal model. *PloS one* 10 (4), e0124657. 10.1371/journal.pone.0124657. [PubMed: 25927436]
- Jin Y, Barnett A, Zhang Y, Yu X, Luo Y, 2017. Poststroke sonic hedgehog agonist treatment improves functional recovery by enhancing neurogenesis and angiogenesis. *Stroke* 48 (6), 1636–1645. 10.1161/STROKEAHA.117.016650. [PubMed: 28487338]
- Lagace DC, Whitman MC, Noonan MA, Ables JL, DeCarolis NA, Arguello AA, Donovan MH, Fischer SJ, Farnbauch LA, Beech RD, DiLeone RJ, Greer CA, Mandyam CD, Eisch AJ, 2007. Dynamic contribution of nestin-expressing stem cells to adult neurogenesis. *The Journal of neuroscience : the official journal of the Society for Neuroscience* 27 (46), 12623–12629. 10.1523/JNEUROSCI.3812-07.2007. [PubMed: 18003841]
- Li L, Harms KM, Ventura PB, Lagace DC, Eisch AJ, Cunningham LA, 2010. Focal cerebral ischemia induces a multilineage cytogenic response from adult subventricular zone that is predominantly gliogenic. *Glia* 58 (13), 1610–1619. 10.1002/glia.21033. [PubMed: 20578055]
- Longa EZ, Weinstein PR, Carlson S, Cummins R, 1989. Reversible middle cerebral artery occlusion without craniectomy in rats. *Stroke*. 20 (1), 84–91 [PubMed: 2643202]
- Luo Y, 2011. Cell-based therapy for stroke. *J. Neural Transm* 118 (1), 61–74. 10.1007/s00702-010-0478-4. [PubMed: 20945074]
- Luo Y, Kuo CC, Shen H, Chou J, Greig NH, Hoffer BJ, Wang Y, 2009. Delayed treatment with a p53 inhibitor enhances recovery in stroke brain. *Annals of neurology* 65 (5), 520–530. 10.1002/ana.21592. [PubMed: 19475672]
- Matsushima GK, Morell P, 2001. The neurotoxicant, cuprizone, as a model to study demyelination and remyelination in the central nervous system. *Brain Pathol.* 11 (1), 107–116 [PubMed: 11145196]
- Mendez AA, Samaniego EA, Sheth SA, Dandapat S, Hasan DM, Limaye KS, Hindman BJ, Derdeyn CP, Ortega-Gutierrez S, 2018. Update in the early management and reperfusion strategies of patients with acute ischemic stroke. *Critical care research and practice* 2018, 9168731. 10.1155/2018/9168731. [PubMed: 30050694]

- Miller AK, Alston RL, Corsellis JA, 1980. Variation with age in the volumes of grey and white matter in the cerebral hemispheres of man: measurements with an image analyser. *Neuropathol. Appl. Neurobiol* 6 (2), 119–132. 10.1111/j.1365-2990.1980.tb00283.x. [PubMed: 7374914]
- Parent JM, 2003. Injury-induced neurogenesis in the adult mammalian brain. *The Neuroscientist : a review journal bringing neurobiology, neurology and psychiatry*. 9 (4), 261–272. 10.1177/1073858403252680. [PubMed: 12934709]
- Powers WJ, Rabinstein AA, Ackerson T, Adeoye OM, Bambakidis NC, Becker K, Biller J, Brown M, Demaerschalk BM, Hoh B, Jauch EC, Kidwell CS, Leslie-Mazwi TM, Ovbiagele B, Scott PA, Sheth KN, Southerland AM, Summers DV, Tirschwell DL, American Heart Association Stroke C, 2018. Guidelines for the early management of patients with acute ischemic stroke: a guideline for healthcare professionals From the American Heart Association/American Stroke Association. *Stroke* 49 (3), e46–e110. 10.1161/STR.000000000000158. [PubMed: 29367334]
- Praet J, Guglielmetti C, Berneman Z, Van der Linden A, Ponsaerts P, 2014. Cellular and molecular neuropathology of the cuprizone mouse model: clinical relevance for multiple sclerosis. *Neurosci. Biobehav. Rev* 47, 485–505. 10.1016/j.neubiorev.2014.10.004. [PubMed: 25445182]
- Seiple BD, Blomgren K, Gimlin K, Ferriero DM, Noble-Haesslein LJ, 2013. Brain development in rodents and humans: Identifying benchmarks of maturation and vulnerability to injury across species. *Progress in neurobiology* 106–107, 1–16. 10.1016/j.pneurobio.2013.04.001.
- Shen H, Luo Y, Kuo CC, Wang Y, 2008. BMP7 reduces synergistic injury induced by methamphetamine and ischemia in mouse brain. *Neuroscience letters* 442 (1), 10.1016/j.neulet.2008.06.052. 15–8. [PubMed: 18598737]
- Spalding KL, Bergmann O, Alkass K, Bernard S, Salehpour M, Huttner HB, Bostrom E, Westerlund I, Vial C, Buchholz BA, Possnert G, Mash DC, Druid H, Frisen J, 2013. Dynamics of hippocampal neurogenesis in adult humans. *Cell* 153 (6), 1219–1227. 10.1016/j.cell.2013.05.002. [PubMed: 23746839]
- Stelman AJ, Thompson JP, Li J, 2012. Demyelination and remyelination in anatomically distinct regions of the corpus callosum following cuprizone intoxication. *Neuroscience research* 72 (1), 32–42. 10.1016/j.neures.2011.10.002. [PubMed: 22015947]
- Sun F, Wang X, Mao X, Xie L, Jin K, 2012. Ablation of neurogenesis attenuates recovery of motor function after focal cerebral ischemia in middle-aged mice. *PLoS one* 7 (10), e46326. 10.1371/journal.pone.0046326. [PubMed: 23110048]
- Tarabozetti A, Walker T, Avila R, Huang H, Caporoso J, Manandhar E, Leeper TC, Modarelli DA, Medicetty S, Shriver LP, 2017. Cuprizone intoxication induces cell intrinsic alterations in oligodendrocyte metabolism independent of copper chelation. *Biochemistry* 56 (10), 1518–1528. 10.1021/acs.biochem.6b01072. [PubMed: 28186720]
- Turcato F, Kim P, Barnett A, Jin Y, Scerba M, Casey A, Selman W, Greig NH, Luo Y, 2018. Sequential combined treatment of pifithrin- α and posiphen enhances neurogenesis and functional recovery after stroke. *Cell transplantation* 27 (4), 607–621. 10.1177/0963689718766328. [PubMed: 29871513]
- Vahid-Ansari F, Lagace DC, Albert PR, 2016. Persistent post-stroke depression in mice following unilateral medial prefrontal cortical stroke. *Translational psychiatry* 6 (8), e863. 10.1038/tp.2016.124. [PubMed: 27483381]
- Ventura-Antunes L, Mota B, Herculano-Houzel S, 2013. Different scaling of white matter volume, cortical connectivity, and gyrfication across rodent and primate brains. *Frontiers in neuroanatomy* 7 (3), 10.3389/fnana.2013.00003.
- Zhang H, Kim Y, Jeoung Ro E, Ho C, Lee D, Trapp BD, Suh H, 2019. Hippocampal neurogenesis and neural circuit formation in a cuprizone-induced multiple sclerosis mouse model. *J. Neurosci* 10.1523/JNEUROSCI.0866-19.2019.

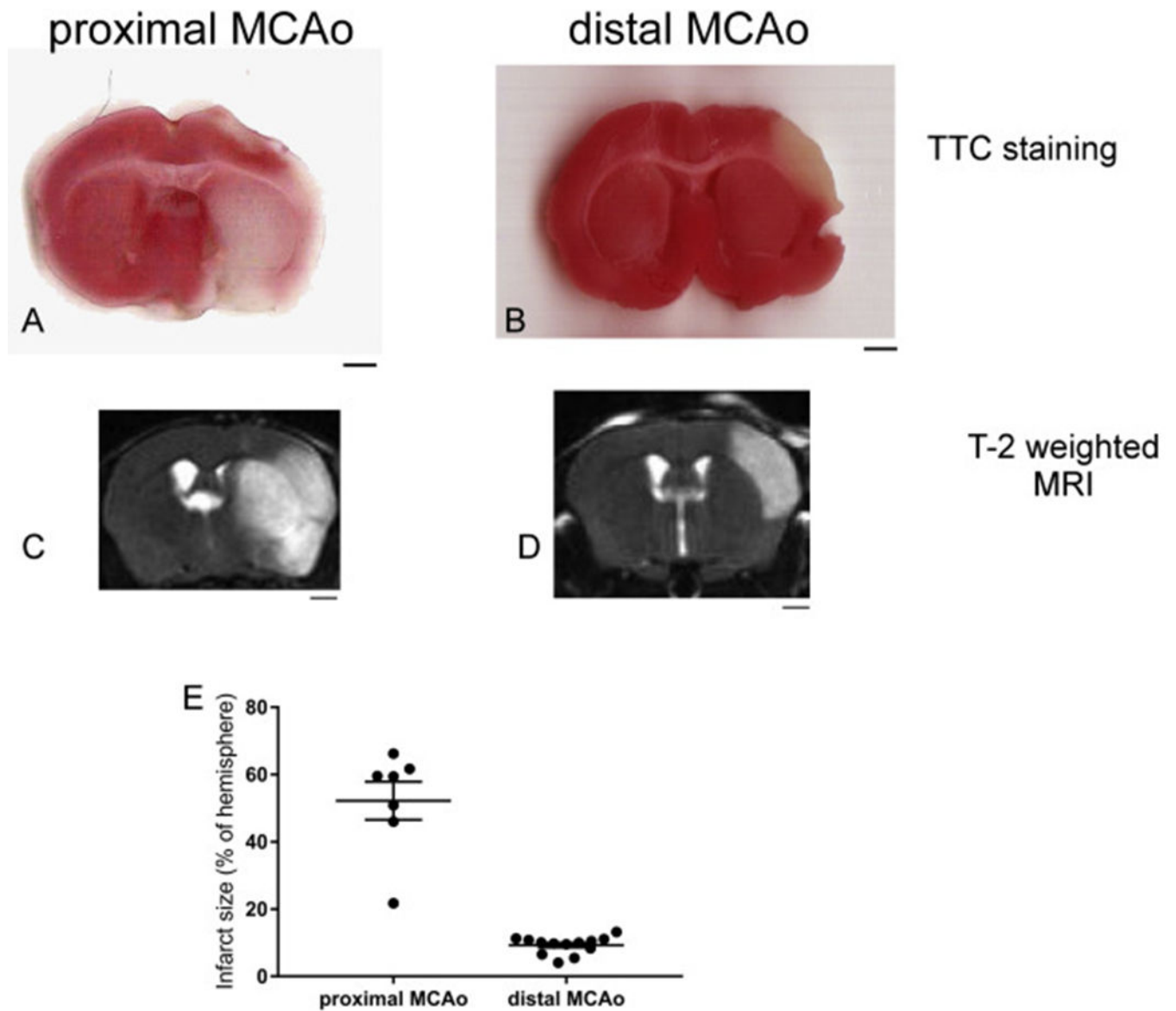


Fig. 1. Proximal MCAo (pMCAo) and distal MCAo (dMCAo) induces different infarct size and locations in mouse brain. (A-B) TTC staining, (C-D) T2-weighted MRI images of pMCAo and dMCAo after 24 h. (E) quantification of infarct size using T2-weighted MRI imaging. The data are presented as MEAN \pm SEM ($n = 7$ for pMCAo and $n = 13$ for dMCAo). Scale bar = 1 mm.

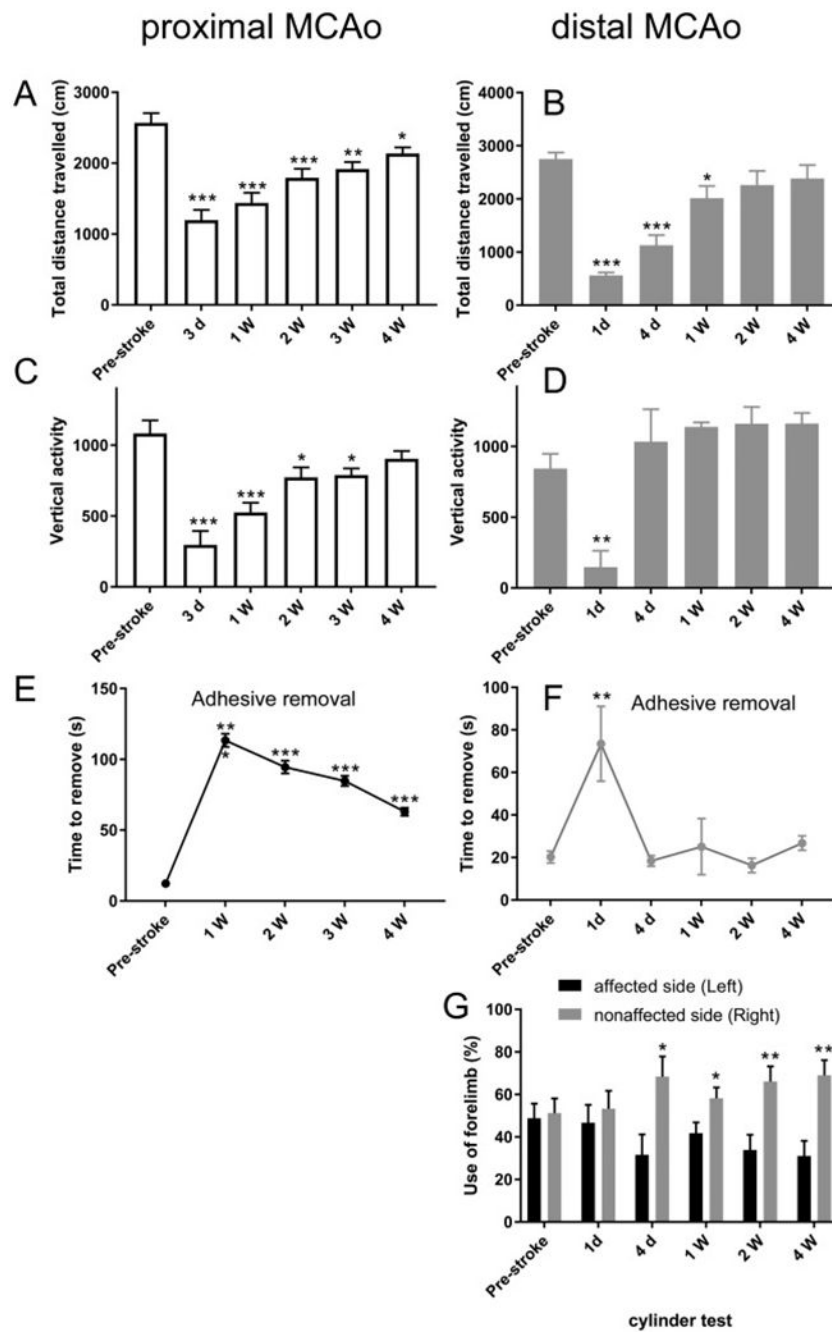


Fig. 2. Behavioral outcomes in pMCAo and dMCAo mice. (A-B) Total horizontal distance traveled, (C-D) Vertical activity, (E-F) Adhesive removal test and (G) Cylinder test results at pre- and post-stroke days. The data are presented as MEAN ± SEM. * p < .05, ** p < .01, and ***p < .001, or. ANOVA. (n = 7 for pMCAo and n = 13 for dMCAo).

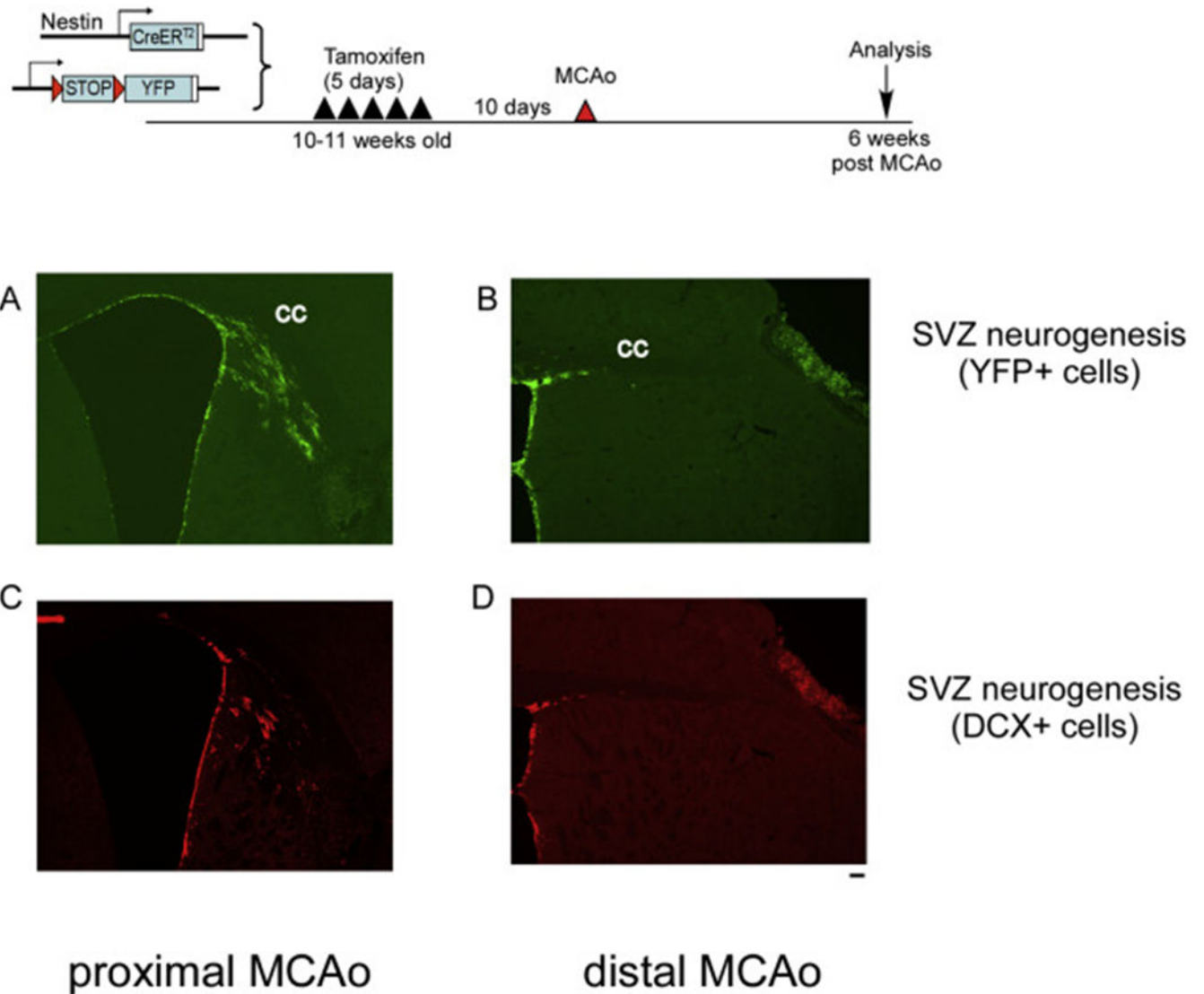
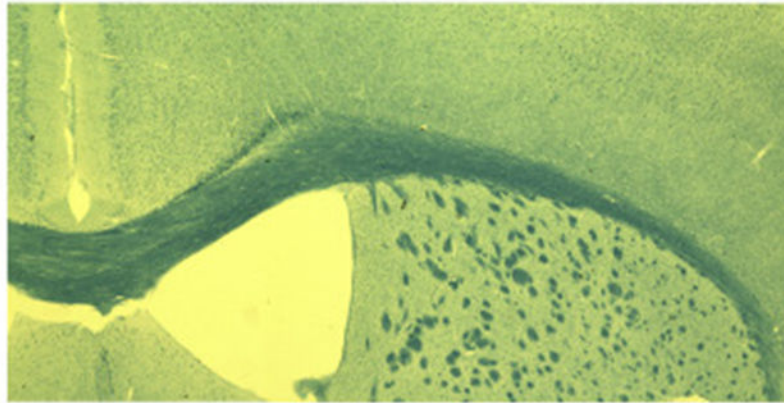
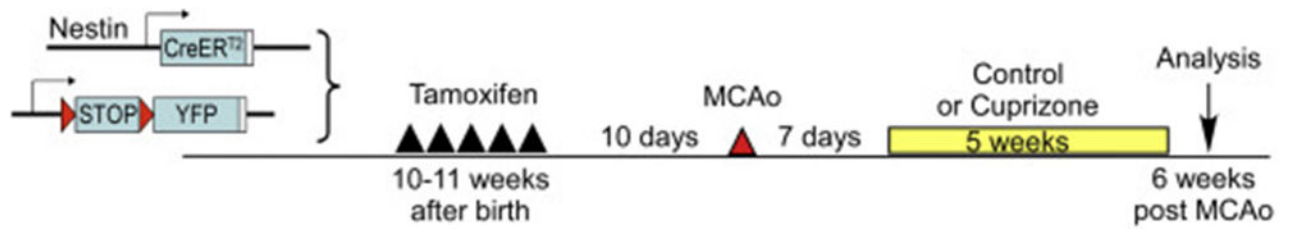
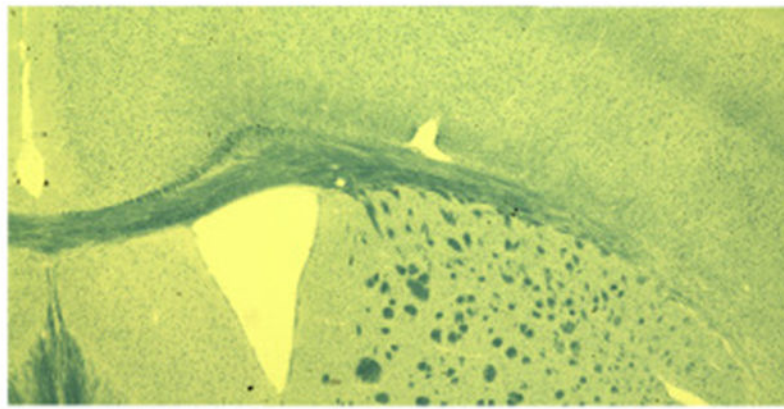


Fig. 3. pMCAo induces more substantial neurogenesis and migration of double cortin (DCX) positive neuroblasts compared to dMCAo. Top panel, experimental timeline. (A-B) YFP+ cells at 6 weeks after pMCAo or dMCAo. (C-D) DCX+ neuroblasts at 6 weeks after pMCAo or dMCAo. Scale bar =100um



Control diet



Cuprizone diet

Fig. 4. Demyelination of corpus callosum following 5-week cuprizone treatment. Luxol fast blue staining in vehicle or cuprizone treated brains. Scale bar =100um. (For interpretation of the references to colour in this figure legend, the reader is referred to the web version of this article.)

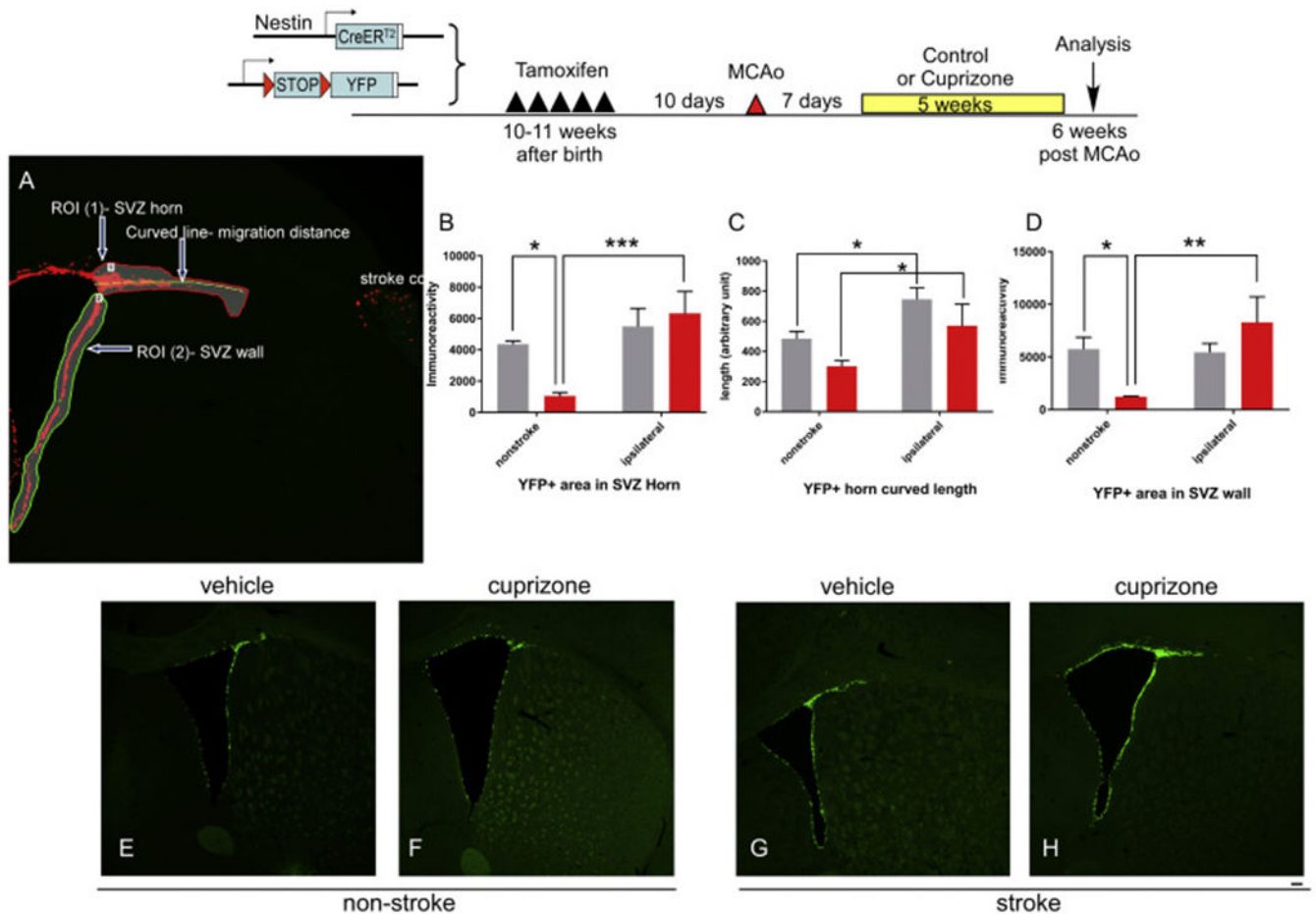


Fig. 5. Effects of Cuprizone treatment on YFP+ cells expansion and migration in non-stroke and stroke mice. Top panel, experimental timeline. A. Illustration of quantification parameters. (B) YFP+ immunoreactive positive cells in the SVZ horn area. (C) migration length of YFP+ cells in SVZ horn area and (D) YFP+ immunoreactive positive cells in the SVZ wall area in different group of mice. (E-H) representative images from each group quantified in B-D. The data are presented as MEAN \pm SEM. * $p < .05$, ** $p < .01$, and *** $p < .001$. ANOVA ($n = 4-5$ for each group). Scale bar = 100 μ m.

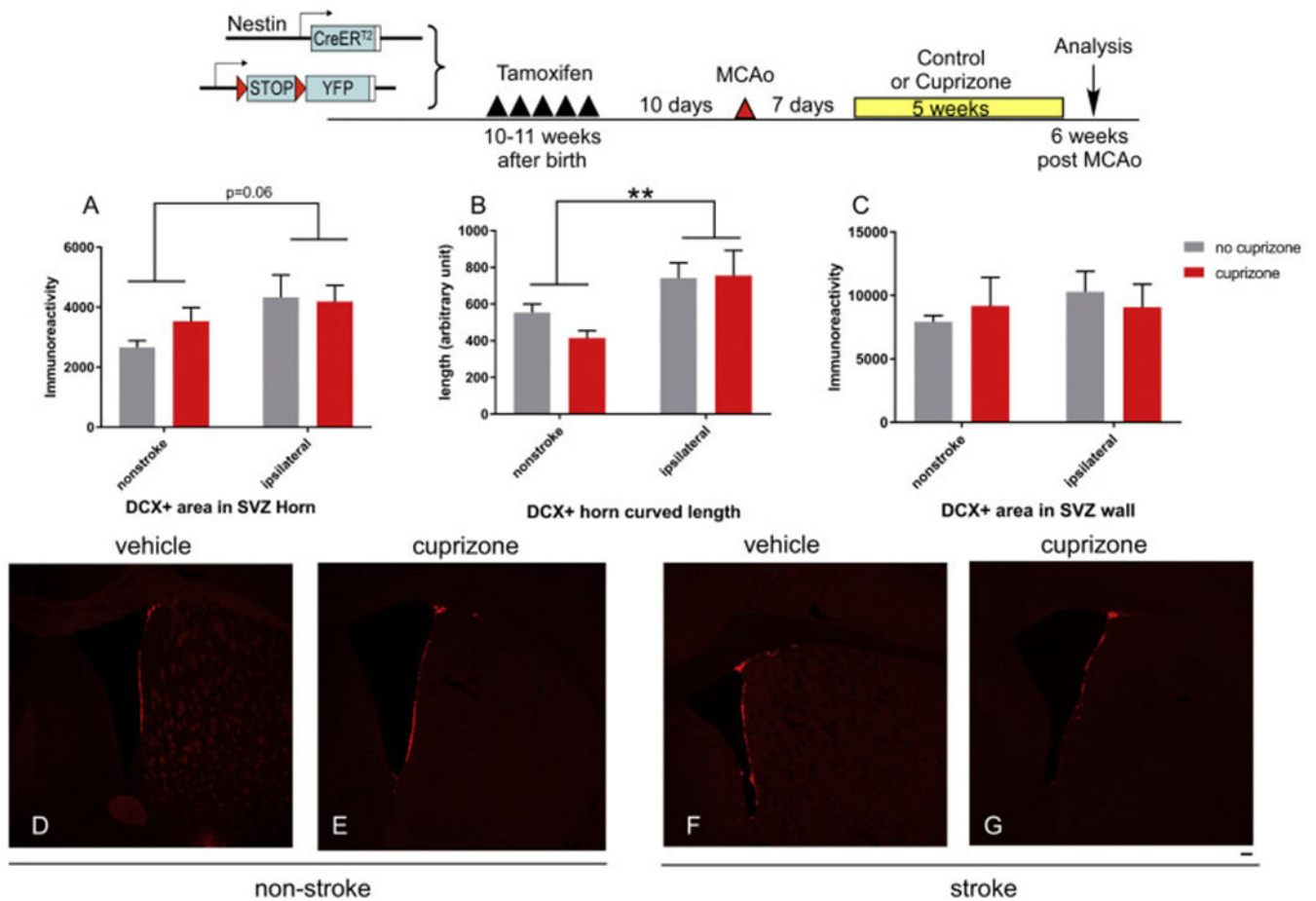


Fig. 6. Effects of Cuprizone treatment on double cortin (DCX) + neuroblast cells expansion and migration in non-stroke and stroke mice. Top panel, experimental timeline. (A) DCX+ immunoreactive positive cells in the SVZ horn area. (B) migration length of DCX+ cells in SVZ horn area and (C) DCX+ immunoreactive positive cells in the SVZ wall area in different group of mice. (D-G) representative images from each group quantified in B-D. The data are presented as MEAN \pm SEM. * $p < .05$, ** $p < .01$, and *** $p < .001$. ANOVA ($n = 4-5$ for each group). Scale bar = 100 μ m.

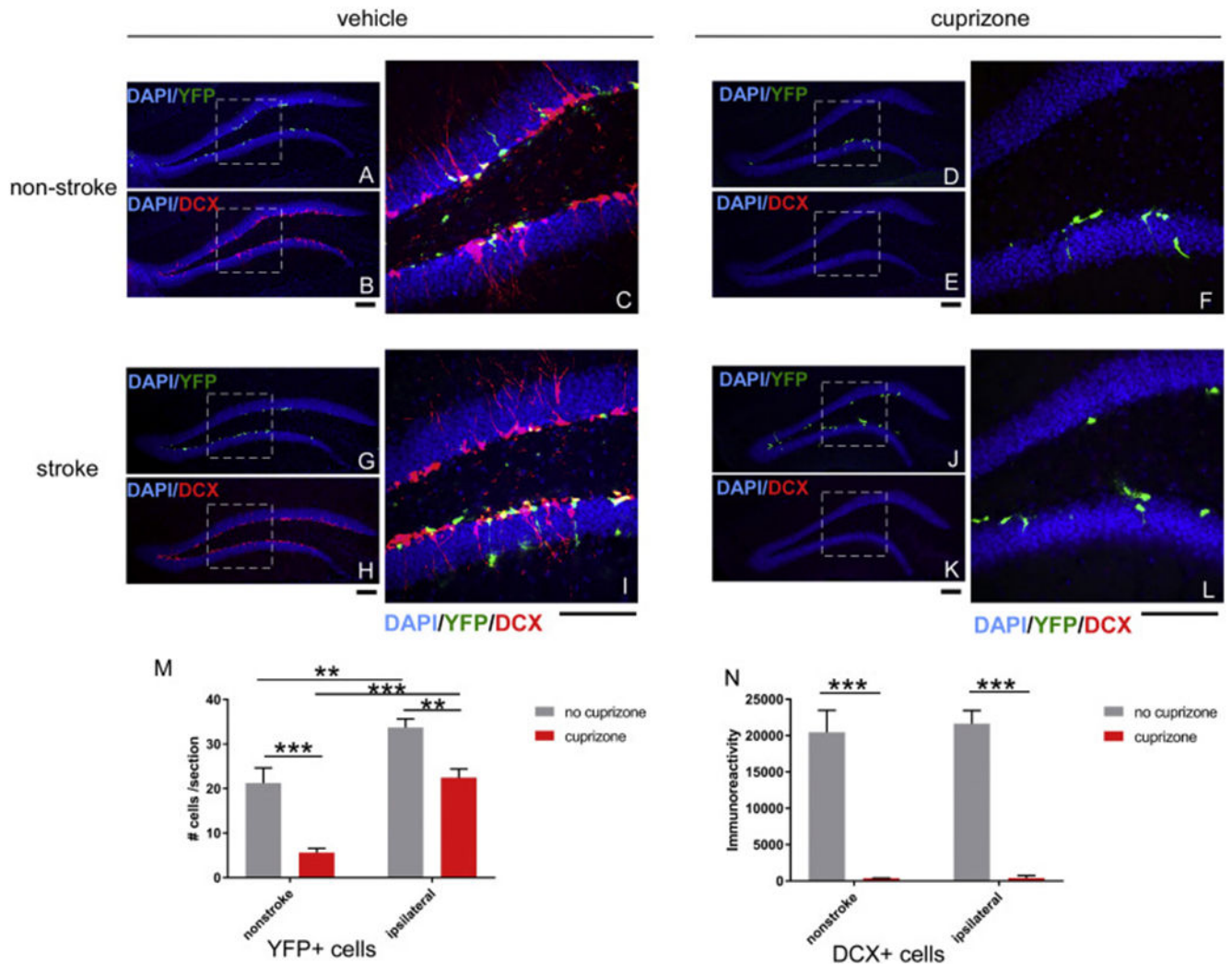


Fig. 7. Effects of Cuprizone treatment on subgranular zone (SGZ) YFP+ and double cortin (DCX) + neuroblast cells expansion and migration in non-stroke and stroke mice. Representative images of YFP+ or DCX+ cells in SGZ from each group (A-C, non-stroke+vehicle; D-F, non-stroke+cuprizone; G-I, stroke+vehicle and J-L, stroke+cuprizone). Dashed square indicate the area that is enlarged in the right panel with higher magnification. All groups are quantified in panel M (YFP+ cells) and panel N (DCX+ cells). The data are presented as MEAN+ SEM. * $p < .05$, ** $p < .01$, and *** $p < .001$. ANOVA ($n = 4-5$ for each group). Scale bar = 100 μ m.

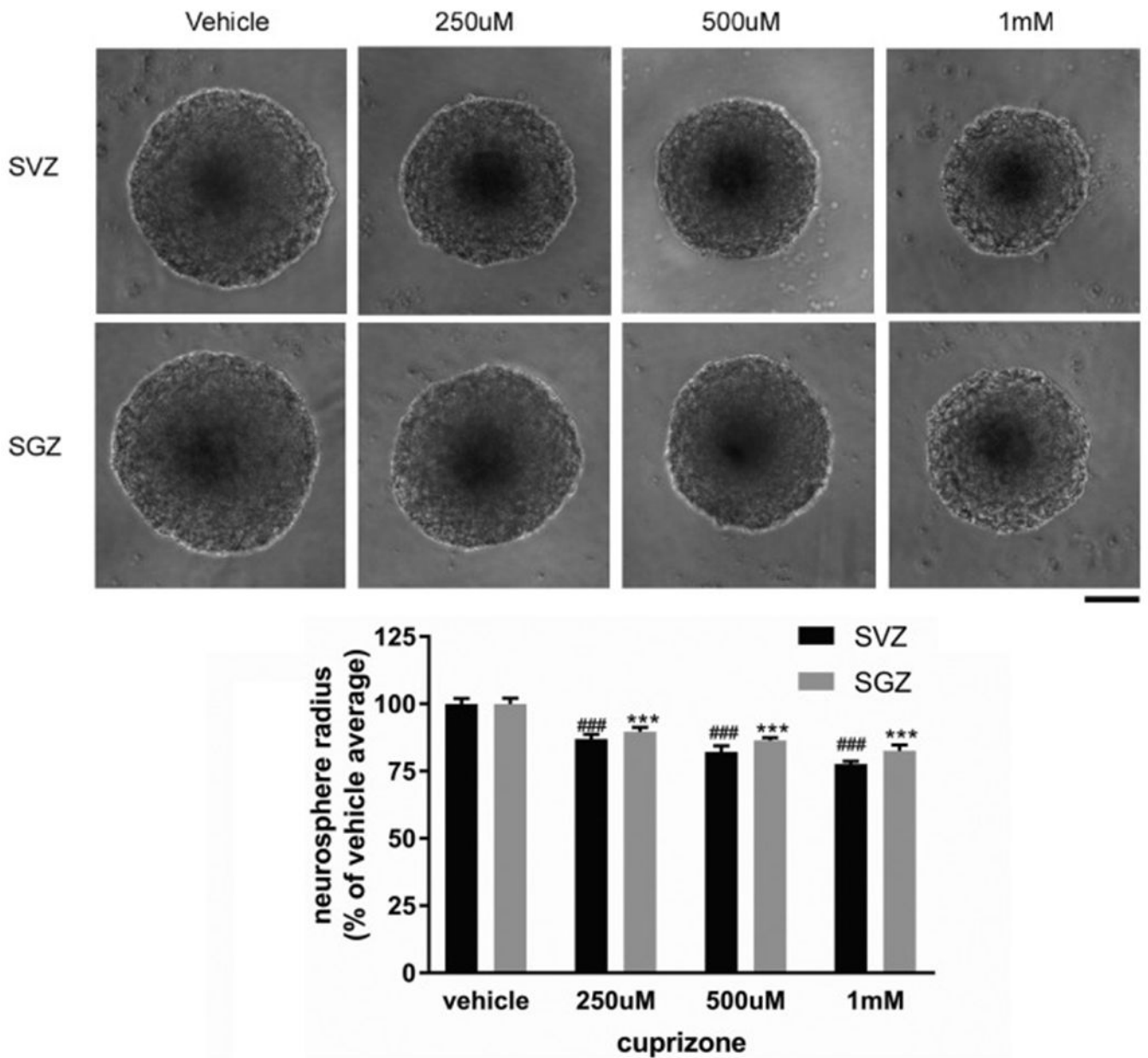


Fig. 8. Direct effects of Cuprizone treatment on SVZ and SGZ neurosphere growth. Representative neurosphere images from different Cuprizone concentration or vehicle treatment initiated at 48-h after cell plating and harvested at 7 days after plating. Quantification of neurosphere radius shown in lower panel. The data are presented as MEAN \pm SEM. ***p < .001. ANOVA (n = 6 for each group). Scale bar = 100um.